THE JOURNAL OF BIOLOGICAL CHEMISTRY VOL. 288, NO. 13, pp. 8862–8874, March 29, 2013

α_3Na$^+$/K$^+$-ATPase Deficiency Causes Brain Ventricle Dilation and Abrupt Embryonic Motility in Zebrafish*[S]

Received for publication, September 21, 2012, and in revised form, February 7, 2013 Published, JBC Papers in Press, February 11, 2013, DOI 10.1074/jbc.M112.421529

Canan Doğanlı[‡§¶], Hans C. Beck[‖], Angeles B. Ribera[**], Claus Oxvig[¶], and Karin Lykke-Hartmann[‡§1]

*From the [‡]Centre for Membrane Pumps in Cells and Disease-PUMPKIN, Danish National Research Foundation, DK-1057 Copenhagen, Denmark, the Departments of [§]Biomedicine and [¶]Molecular Biology and Genetics,Aarhus University, DK-8000 Aarhus, Denmark, the [‖]Department of Clinical Biochemistry and Pharmacology, Centre for Clinical Proteomics, Odense University Hospital, DK-5000 Odense, Denmark, and the **Department of Physiology and Biophysics, University of Colorado Denver, Anschutz Medical Campus, Aurora, Colorado 80045*

Background: The Na$^+$/K$^+$-ATPase maintains Na$^+$/K$^+$ gradients across the plasma membrane, essential for cellular functions.
Results: Zebrafish deficient of α_3Na$^+$/K$^+$-ATPase display abnormal motility and brain ventricle dilation.
Conclusion: Zebrafish α_3Na$^+$/K$^+$-ATPase is CNS-specific and required for brain ventricle maintenance and embryonic motility.
Significance: This is the first study assessing α_3Na$^+$/K$^+$-ATPase in brain development and embryonic motility.

Na$^+$/K$^+$-ATPases are transmembrane ion pumps that maintain ion gradients across the basolateral plasma membrane in all animal cells to facilitate essential biological functions. Mutations in the Na$^+$/K$^+$-ATPase α_3 subunit gene (*ATP1A3*) cause rapid-onset dystonia-parkinsonism, a rare movement disorder characterized by sudden onset of dystonic spasms and slow movements. In the brain, *ATP1A3* is principally expressed in neurons. In zebrafish, the transcripts of the two *ATP1A3* orthologs, *Atp1a3a* and *Atp1a3b*, show distinct expression in the brain. Surprisingly, targeted knockdown of either *Atp1a3a* or *Atp1a3b* leads to brain ventricle dilation, a likely consequence of ion imbalances across the plasma membrane that cause accumulation of cerebrospinal fluid in the ventricle. The brain ventricle dilation is accompanied by a depolarization of spinal Rohon-Beard neurons in *Atp1a3a* knockdown embryos, suggesting impaired neuronal excitability. This is further supported by *Atp1a3a* or *Atp1a3b* knockdown results where altered responses to tactile stimuli as well as abnormal motility were observed. Finally, proteomic analysis identified several protein candidates highlighting proteome changes associated with the knockdown of *Atp1a3a* or *Atp1a3b*. Our data thus strongly support the role of α_3Na$^+$/K$^+$-ATPase in zebrafish motility and brain development, associating for the first time the α_3Na$^+$/K$^+$-ATPase deficiency with brain ventricle dilation.

The Na$^+$/K$^+$-ATPase is essential for maintaining Na$^+$ and K$^+$ gradients across the plasma membrane, required for many cellular functions, *e.g.* regulation of cell volume, pH, Na$^+$-coupled secondary transport of molecules and neurotransmitters, and the excitability of muscle and neuronal cells (1, 2). In mammals, the four α (α_1, α_2, α_3, and α_4) isoforms display distinct tissue-specific expression patterns (2, 3). The α_3 isoform (ATP1α_3) is expressed in brain, eye, ear, muscle, cartilage, uterus, placenta, and heart (4–7). In the brain, the ATP1α_3 subunit is present exclusively in neurons (8). Mutations in the gene cause the neurological disorder rapid-onset dystonia-parkinsonism (RDP)[2] (9, 10), a rare movement disorder with an abrupt onset and rapid (hours to weeks) development of dystonia parkinsonism, primarily bradykinesia and postural instability (10, 11).

Besides ion pump roles, Na$^+$/K$^+$-ATPases also serve as signal transducers, modulating synaptic plasticity, *e.g.* inducing dendritic growth in cortical neurons (12). Evidence for neuronal roles of ATP1α_3 was previously found in both human and rat dorsal root ganglia and also observed in rat embryos (embryonic day 21) (13).

Currently, two different genetically modified mouse models targeting the *Atp1a3* gene exist: $\alpha_3{}^{+/-}\mathrm{KI}_{I4}$ (14) and $\alpha_3{}^{+/-}\mathrm{KI}_{I810N}$ (Myshkin) (15). These mice display learning/memory deficits (14), epilepsy/seizures (15), stress-induced motor symptoms (16), anxious phenotype, and depression-like behavior (17). However, they do not fully capture the human RDP symptoms, and the pathology of RDP remains unsolved.

Recently, it became more evident that *Danio rerio* (zebrafish) is a valuable model for investigating Na$^+$/K$^+$-ATPase functions (18, 19). We employed zebrafish, with its advantageous properties, *e.g.* external development with optical clarity, small size, short generation time (2–3 months), and high fecundity (20, 21) to further study the role of ATP1α_3 in early neuronal functions.

* This work was supported by grants from Aarhus University Forskningsfond (AUFF), and Danish National Research Foundation (DNRF) (Centre for Membrane Pumps in Cells and Disease (PUMPKIN)) (DNRF85).
[S] This article contains supplemental Tables S1 and S2 and Movies 1–4.
[1] To whom correspondence should be addressed: Dept. of Biomedicine and Centre for Membrane Pumps in Cells and Disease, Aarhus University, Ole Worms Alle 3, DK-8000, Aarhus C, Denmark. Tel.: 45-8716-7802; Fax: 45-8613-1160; E-mail: kly@biokemi.au.dk.

[2] The abbreviations used are: RDP, rapid-onset dystonia-parkinsonism; KD, knockdown; RB, Rohon-Beard; RMP, resting membrane potential; MO, morpholino oligonucleotide; std-MO, standard control MO; SP-MO, splicing MO; Tg, transgenic; qRT-PCR, quantitative RT-PCR; iTRAQ, isobaric tags for relative and absolute quantitation; DA, dopaminergic; TH, tyrosine hydroxylase; L-DOPA, L-3,4-dihydroxyphenylalanine; CSF, cerebrospinal fluid; hpf, hours postfertilization; Prim, primordium of the lateral line.

In a comparison of the zebrafish brain structure with human, the gross architecture of many zebrafish brain areas, *e.g.* retina, olfactory bulb, hypothalamus, cerebellum, and spinal cord, is similar to that of humans, although there exist some differences between teleosts and mammals (22). Moreover, zebrafish enables several behavioral and drug tests and hence is relevant for many disease-related studies.

Zebrafish have two *ATP1A3* orthologs, *Atp1a3a* and *Atp1a3b* (23). Surprisingly, knockdown (KD) of *Atp1a3a* or *Atp1a3b* results in severe brain ventricle dilation in contrast to previous data, where KD of *Atp1a1* caused reduced brain ventricle inflation (33), thus supporting the role of Na^+/K^+-ATPase in brain ventricle development. The brain ventricle dilation in *Atp1a3a/b* KD embryos was accompanied by an ~20-mV depolarization of the spinal Rohon-Beard (RB) neuron resting membrane potential (RMP), suggesting compromised functions in neurons as a consequence of *Atp1a3a* KD-generated defects in ion homeostasis. In support of this, morphant embryos further displayed both abnormal touch response and spontaneous movements. To identify additional neuronal functions that may depend on correct ion homeostasis for normal performance, we used a proteomic approach. Interestingly, this revealed several proteins, including cytoskeletal, ion-binding, muscle-associated proteins, etc., with expression levels that were affected by *Atp1a3a* or *Atp1a3b* KD.

This is the first detailed study of α_3Na^+/K^+-ATPases in zebrafish and on the basis of conservation of zebrafish and mammalian α_3Na^+/K^+-ATPase expression and functions. Zebrafish can serve as an advantageous model for analysis of brain ventricular volume maintenance and embryonic motility, both related to ion homeostasis.

EXPERIMENTAL PROCEDURES

Animals—TU (Tübingen) zebrafish strain (Nüsslein-Volhard Laboratory, Max Planck Institute, Tübingen, Germany) and Tg(gfap:GFP) transgenic line (Zebrafish International Resource Center, University of Oregon) of either sex were used in the experiments. Embryo maintenance and staging were performed as described previously (24, 25). To conserve optical clarity, embryos were raised in the presence of 0.2 mM 1-phenyl-2-thiourea (24).

Reverse Transcription (RT) and qRT-PCR— qRT-PCR protocol was performed on cDNAs from embryos at corresponding stages (1000-cell, 50% epiboly, 75% epiboly, 6-somite, prim-6, prim-22, pectoral fin, and adult (one male + one female)) as described previously (26). Pearl Primer software (27) and Roche Applied Science assay design were used to design the primers (supplemental Table S2) to detect transcripts of *Atp1a3a* (accession number: NM_131684.2), *Atp1a3b* (accession number: NM_131685.2), *Actb2* (accession number: NM_181601.3), and *Bhmt*, *Ckma*, *Ckmb*, *Gamt*, *Gpib*, *Krt4*, *Krt5*, *Mhyz2*, *Ndpkz2*, *Pgam2*, *Pvalb9*, *Zgc:91930*, and *113d7.4*, accession numbers of which are provided in Table 1. Generated PCR product sizes and identities were verified by gel electrophoresis (data not shown) and DNA sequencing.

To investigate SP-MO-mediated KD, we initially performed RT-PCR using primers enclosing the presumably extruded exons. This clearly indicated that both SP-MOs caused a KD via nonsense-mediated mRNA decay (data not shown). The quantitation of KD levels was performed by qRT-PCR on first strand cDNA generated from ~30 WT, std-MO- (5.5, 11, and 3 ng), α_{3a}-SP-MO- (5.5 and 11 ng), and α_{3b}-SP-MO- (1.5 and 3 ng) injected embryos.

Efficiency of each primer pair used in qRT-PCR was detected to be ~100%. Transcription levels were quantified using the relative quantification method based on comparative threshold cycle values (C_t).

Cloning of Zebrafish Atp1a3a and Atp1a3b cDNA—Total RNA was isolated from a male and a female zebrafish by the TRIzol® method (Invitrogen) (28). Total RNA was used as template to perform RT-PCR by using the SuperScript™ III RT-PCR system (Invitrogen) according to the manufacturer's instructions with *Atp1a3a*- and *Atp1a3b*-specific primer pairs (supplemental Table S2) tagged with restriction enzyme recognition sites. The program for RT-PCR was one cycle for 30 min at 55 °C and 2 min at 94 °C followed by 40 cycles of 15 s at 94 °C, 30 s at 66 °C, and 4 min at 68 °C and a final extension for 15 min at 68 °C. Gel-purified RT-PCR fragments were cloned into pTZ57R vector (InsTAclone™ PCR cloning kit, Fermentas) following the manufacturer's protocol and subsequently subjected to DNA sequencing.

In Situ Hybridization and Sectioning—Antisense and sense RNA probe templates were generated by PCR on pTZ57R vector harboring *Atp1a3a* probe coding sequence, for *Atp1a3a*, and by RT-PCR on adult zebrafish RNA, for *Atp1a3b*, introducing a T7 priming site in both scenarios. Probes were digoxigenin-labeled during synthesis from purified PCR products by using the digoxigenin RNA labeling mix (Roche Applied Science) and T7 polymerase (Roche Applied Science) following the manufacturer's protocol. Embryos were fixed overnight in freshly prepared 4% paraformaldehyde in phosphate-buffered saline (PBS, pH 7.4) and kept in MetOH in −20 °C. To detect *Atp1a3a* and *Atp1a3b* transcripts, whole-mount *in situ* hybridization was performed on embryos at 60 hpf, as described previously (29) with minor modifications.

Embryos were embedded and oriented in 5% agar so that they could be cut transversely following dehydrating in ascending alcohol solutions (70% ×2, 96% ×2, and 99% ×2), infiltration, and embedding in glycolmethacrylate (Technovit 7100). Using a Microm 355, 20-μm-thick sections were cut, and every 10th section was taken by systematic sampling. Whole-mount embryos and sections were observed using an inverted microscope, Olympus IX71.

MO-mediated Knockdown of Atp1a3a or Atp1a3b and mRNA Rescue—MOs (Gene Tools, LLC) for microinjection were diluted in distilled water and microinjected into embryos at the 1–4 cell stage. Translation-blocking MOs were: α_{3a}-MO (5′-CTTTCTTCAGTCTGTCAAACGGCGT-3′) (12 ng) and α_{3b}-MO (5′-AGAGTGATGGAGAAAGTGACAGCCT-3′) (3 ng); the splice-blocking MOs were: α_{3a}-SP-MO (5′-TCCACCTGAGCAATGACACCAAACA-3′) (11 ng), targeting the intron 6-exon 7 boundary, and α_{3b}-SP-MO (5′-AGTGCCTGACAGAAACAAAGCATTT-3′) (3 ng), targeting the intron 7-exon 8 boundary. The standard control MO (std-MO: 5′-CCTCTTACCTCAGTTACAATTTATA-3′) (3 and 12 ng) and the p53-MO (5′-GCGCCATTGCTTTGCAAGAATTG-

3′) (4 ng) were injected at the indicated amounts. Embryos were grown for 60 h in embryo medium with 0.003% 1-phenyl-2-thiourea and observed under an inverted microscope, Olympus IX71. To visualize zebrafish brain ventricles, rhodamine-conjugated dextran was injected into the brain ventricle at 48 hpf as described previously (30), and embryos were subsequently imaged under bright field and fluorescent light (Olympus IX71).

The template for *Atp1a3a* and *Atp1a3b* mRNA was generated by PCR on pTZ57R vector harboring *Atp1a3a* (3069 bp) and *Atp1a3b* (3069 bp) coding sequences. *In vitro* synthesis of *Atp1a3a* and *Atp1a3b* mRNA was performed on gel-purified *Atp1a3a* and *Atp1a3b* PCR products by using the mMESSAGE mMACHINE T7 ULTRA kit (Ambion) following the manufacturer's instructions. The RNA products were gel-purified (Qiagen), and each embryo was co-injected with 180 pg of WT *Atp1a3a* mRNA or 45 pg of WT *Atp1a3b* mRNA together with 11 ng of α_{3a}-SP-MO or 3 ng of α_{3b}-SP-MO, respectively. Embryos were assessed at 60 hpf, grouped morphologically into three classes depending on the severity of the brain ventricle dilation (+, slight/no; ++, moderate; +++, severe) (see Fig. 2*D*, *lower panel*), and quantified as percentages of the total number of embryos. Experiments were repeated at least three times, and data are presented as mean ± S.D.

Atp1a3a RNA in Situ Hybridization and TH Immunostaining—WT TU zebrafish were raised in embryo medium with 1-phenyl-2-thiourea. RNA *in situ* hybridization was adapted from Schulte-Merker *et al.* (31), and immunostaining was subsequently performed as described previously (29) with minor modifications. *In situ* hybridization was applied on noninjected embryos using *Atp1a3a* antisense riboprobe, and the final labeling was maintained by Fast Red tablets (Sigma). Stained embryos were fixed in 4% paraformaldehyde, blocked in 10% heat inactivated goat serum/phosphate buffered saline (PBS)/0.1% Tween20 (HIGS/PBST), and incubated in anti-TH primary antibody (Millipore) at 1:200 final concentration overnight at 4 °C. Following the washes, embryos were incubated in goat anti-mouse secondary antibody conjugated to Alexa Fluor 488 at 1:1000 final concentration, for 4 h at room temperature. After serial washings, embryos are gradually transferred to 100% glycerol and imaged under Leica DM4000 and Zeiss LSM 710 T-PMT confocal microscope upon being mounted in 0.5% agarose at proper orientation.

Quantification of DA Neurons—Tyrosine hydroxylase (*Th*) antisense riboprobe was generated as *Atp1a3b* riboprobe, described above. *In situ* hybridization protocol to detect *Th* mRNA expression, applying labeling via Fast Red tablets, was adapted from Schulte-Merker *et al.* (31) and performed on WT, α_{3a}-SP-MO-mediated *Atp1a3a* KD, and *Atp1a3a* mRNA-rescued *Atp1a3a* KD embryos. Embryos were observed under an inverted microscope, Olympus IX71. Bright field images of *Th* riboprobe hybridized WT ($n = 10$) and α_{3a}-SP-MO-mediated *Atp1a3a* KD embryos ($n = 10$) were quantified in terms of dopaminergic (DA) neuron content. Due to the extent of the brain ventricle dilation, it was not possible to quantify the number of DA neurons by single-cell count, and thus, total staining of labeled DA neurons in these embryos was quantified using a semiquantitative open source image analysis software, ImageJ (National Institutes of Health, Bethesda, MD). Mean integrated density ± S.D. was plotted.

Whole-cell Patch Clamp Electrophysiology for Atp1a3a—*Atp1a3a* KD and control embryos at 48 hpf were sacrificed, skinned, and mounted dorsally to enable access to RB cells as described previously (32). *Atp1a3a* KD embryos were grouped into two groups according to brain ventricle dilation severity: ones with severe dilation (+++) and ones with slight/no (+) dilation. Electrodes were made to a tip resistance of 2.6–3.7 megaohms using a P-97 microelectrode puller (Sutter Instruments, Novato, CA) and filled with intracellular pipette solution (in mM: 135 KCl, 10 EGTA, and 10 HEPES; pH 7.4). RMP recordings were obtained from RB cells of these embryos together with WT and std-MO-injected control embryos using patch electrodes and an Axopatch-200B amplifier (Axon Instruments, Molecular Devices, Sunnyvale, CA). Recordings were performed at room temperature, using bath solution (in mM: 125 NaCl, 3 KCl, 10 $CaCl_2$, and 5 HEPES; pH 7.4) under an inverted microscope, Zeiss Axioskop (Germany). Data are presented as mean ± S.E.

Touch Response—Mechanosensory stimulation was delivered to the embryo trunk with a needle. WT, std-MO-injected, α_{3a}-MO-injected, and α_{3b}-MO-injected embryos with brain ventricle dilation phenotype at 60 hpf were recorded under an Olympus IX71 microscope at 25 frames/s. Experiments were independently repeated at least three times.

Proteomics Analysis by Isobaric Tags for Relative and Absolute Quantitation (iTRAQ)—30–50 of std-MO-, α_{3a}-MO-, and α_{3b}-MO-injected embryos, 60 hpf, were collected in Eppendorf tubes and lysed in lysis buffer (0.02 M Tris, 0.137 M NaCl, 1% Nonidet P-40, 10% glycerol, 1 mM PMSF, 1× Complete protease inhibitor mixture tablet (Roche Applied Science)) with the help of a homogenizer. Cell lysate was analyzed by iTRAQ LC-MS/MS as described previously (33). Briefly, the cell lysate was in-solution-digested using trypsin and labeled with the iTRAQ (reporter ions m/z 114 and 115) followed by fractionation of the peptide mixture using hydrophilic interaction chromatography and LC-MS/MS analysis of the peptide fractions. Raw data files were processed using the Proteome Discoverer software (version 1.3) integrated with the MASCOT database search program (version 2.2.3). Data were searched against the Non-redundant Database (nrDB) restricted to *D. rerio*.

RESULTS

Specific Expression of Atp1a3a and Atp1a3b Transcripts in the Developing Zebrafish Brain—As an initial step to understand the roles of the α_3Na^+/K^+-ATPases, we assessed expression of *Atp1a3a* and *Atp1a3b* mRNA by qRT-PCR. We detected the *Atp1a3a* transcript at the 1000-cell (3 hpf) and 50% epiboly (5.3 hpf) stages. Thereafter it declined and was barely detectable by 75% epiboly (8 hpf) and at the 6-somite (12 hpf) stage, suggesting that these early detected transcripts were provided maternally. *Atp1a3a* reappeared at the prim-6 (25 hpf) and prim-22 (35 hpf) stages. The highest expression of *Atp1a3a* occurred at the pectoral fin stage (60 hpf), which was almost 6-fold higher than the relative expression of the *Atp1a3a* transcript in adult zebrafish (Fig. 1*A*). In contrast, the *Atp1a3b* mRNA was barely detectable from the 1000-cell to

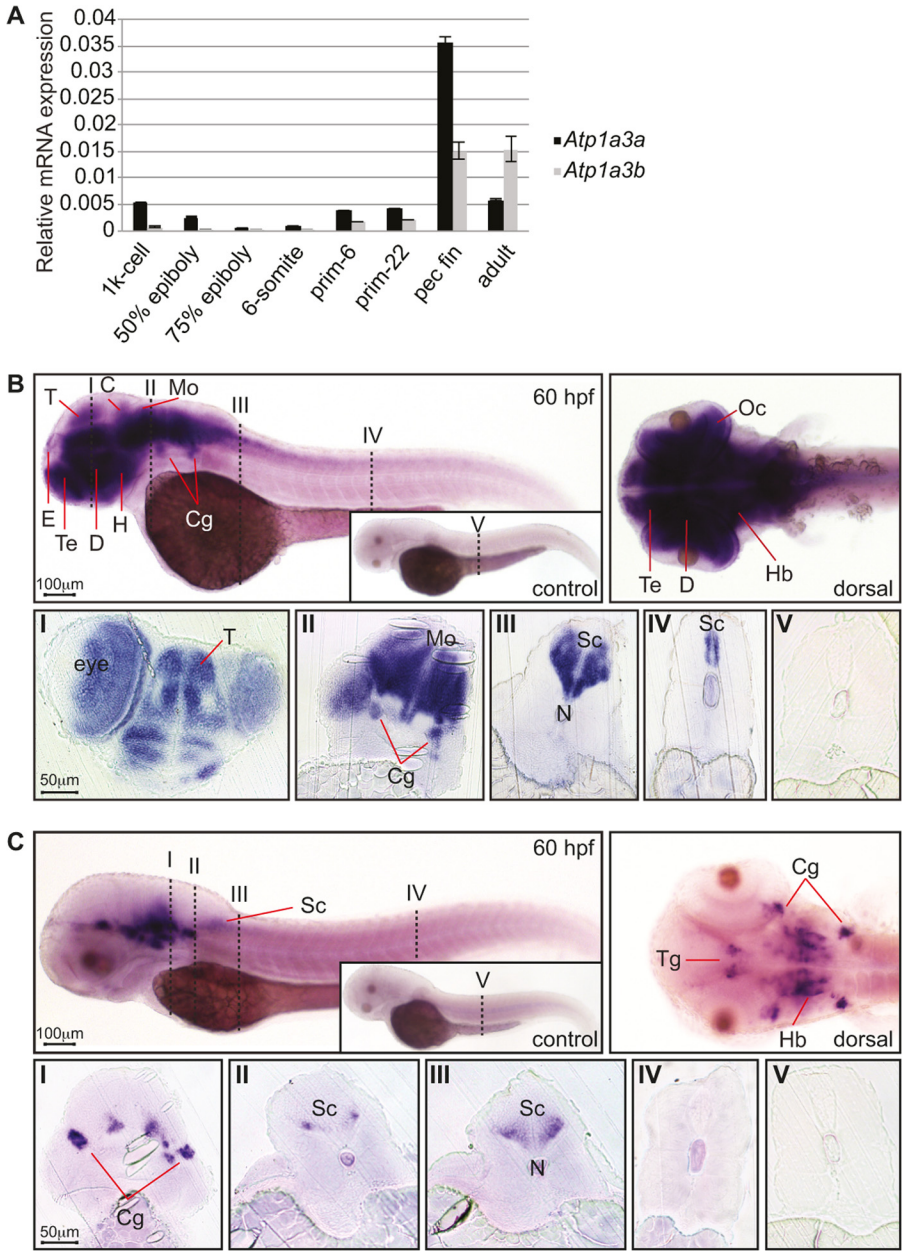

FIGURE 1. **Expression of *Atp1a3a* and *Atp1a3b* mRNA in zebrafish embryos.** *A*, *Atp1a3a* (*black bars*) and *Atp1a3b* (*gray bars*) mRNA expressions were quantified by qRT-PCR and normalized to *Actb2* expression. Data are presented as mean ± S.E. of triplicate measurements. *B*, *Atp1a3a* mRNA expression analyzed by whole-mount *in situ* hybridization in 60 hpf zebrafish embryos; the *inset* shows sense probe hybridized control embryo. *Atp1a3a* is expressed in the brain and the spinal cord. The *numbered vertical dashed lines*, here and in *C*, show the positions of the transverse sections shown below in *sections I–V*. The abbreviations used are: *C*: cerebellum; *Cg*: cranial ganglia; *D*: diencephalon; *E*: epiphysis; *H*: hypothalamus; *Hb*: hindbrain; *Mo*: medulla oblongata; *N*: notochord; *Oc*: optic cup; *T*: tectum; *Te*: telencephalon; *Tg*: tegmentum; *Sc*: spinal cord. *Scale bars* represent 100 μm in whole-mount images and 50 μm in sections. *C*, *Atp1a3b* mRNA expression analyzed by whole-mount *in situ* hybridization in 60 hpf zebrafish embryos; the *inset* shows sense probe hybridized control embryo. *Atp1a3b* is expressed in specific brain regions.

the 6-somite stage (Fig. 1*A*), suggesting lack of maternal *Atp1a3b* contribution. Similar to *Atp1a3a*, the *Atp1a3b* transcript appeared at prim-6 and onwards and also showed a marked increase at the pectoral fin stage (Fig. 1*A*). Further experiments were performed at 48–60 hpf due to the notable expression of both isoforms at these stages and the fact that the embryonic central nervous system (CNS) is well structured by these stages. At these time points, the MO is still effective.

To determine whether of *Atp1a3a* and *Atp1a3b* transcripts were present in the CNS, we then performed *in situ* hybridization. The lack of antibody that detects the zebrafish α_3 isoforms did not allow us to directly test protein levels; however, we assume that the detected transcripts give rise to protein products and represent active Na^+/K^+-ATPase pumps in the plasma membrane of the cell.

We showed that *Atp1a3a* transcripts localize to several CNS structures, including the epiphysis, tegmentum, tectum, cerebellum, cranial ganglia, hindbrain, and spinal cord (Fig. 1*B*). A dorsal view of the head shows a dense accumulation of the *Atp1a3a* transcript throughout the brain. Transverse rostral sections illustrate in more detail *Atp1a3a* expression in several brain structures (Fig. 1*B*, *section I*). More caudal sections show *Atp1a3a*

expression in different CNS regions including the cranial ganglia (Fig. 1*B*, *section II*) and spinal cord (Fig. 1*B*, *sections III* and *IV*).

In contrast to the widespread expression of *Atp1a3a*, the *Atp1a3b* transcript was detected in a more restricted but overlapping set of brain structures such as epiphysis, tegmentum, cranial ganglia, hindbrain and anterior spinal cord, evident in both lateral and dorsal views (Fig. 1*C*). Transverse sections show *Atp1a3b* expression in the hindbrain and cranial ganglia (Fig. 1*C*, *sections I* and *II*), in the rostral (Fig. 1*C*, *section III*) but not the caudal (Fig. 1*C*, *section IV*) spinal cord.

Knockdown of Atp1a3a Causes Brain Ventricle Dilation—To test for a role of the $\alpha_{3a}Na^+/K^+$-ATPase in zebrafish development, we used an antisense MO oligonucleotide-mediated KD approach. The translation-blocking MOs inhibit protein synthesis by binding to the translation initiation site, whereas the splice-blocking MOs bind to intron-exon boundaries and may inhibit proper splicing of the corresponding pre-mRNA, causing nonsense-mediated mRNA decay. In both MO approaches, we assume that the protein function is significantly reduced. The efficiency of *Atp1a3a* KD induced by α_{3a}-SP-MO was determined by qRT-PCR, demonstrating up to 62% reduction in the *Atp1a3a* transcript with increasing MO concentration (Fig. 2*C*).

Marked brain ventricle dilation was observed upon KD of *Atp1a3a* using either translation-blocking (α_{3a}-MO) or splice-blocking (α_{3a}-SP-MO) MOs (Fig. 2*A*), and was further visualized by rhodamine-conjugated dextran injection into zebrafish brain ventricles (Fig. 2*B*). Use of the transgenic line, Tg(gfap: GFP), that expresses green fluorescent protein (GFP) in astrocytes provided an overall view of the CNS structure. A pressure to the brain structures from the ventricle dilation was evident upon *Atp1a3a* KD (Fig. 2*B*). Injection of α_{3a}-SP-MO led to severe, moderate, or slight/no brain ventricle dilation in 54, 36, or 11% of embryos, respectively (Fig. 2*D*), whereas std-MO-injected embryos appeared morphologically normal (Fig. 2*A*).

To exclude that the observed brain ventricle dilation was caused by nonspecific MO-induced activation of p53-dependent apoptosis (34), control experiments were carried out. Co-injection of p53-MO with any of the MOs did not have an effect on the phenotype (Fig. 2*A*), suggesting that p53-dependent effects, *e.g.* apoptosis, did not cause the phenotypes of *Atp1a3a* KD. To further confirm the specificity of the *Atp1a3a* KD phenotypes, embryos were co-injected with *in vitro*-synthesized *Atp1a3a* mRNA. In the rescued embryos, the extent of the brain ventricle dilation was reduced as compared with *Atp1a3a* KD embryos, and severe, moderate, and slight/no ventricle dilation was present in 21, 29, and 50%, respectively (Fig. 2*D*). Taken together, these findings suggest that *Atp1a3a* KD had specific effects that led to the brain ventricle dilation in α_{3a}- and α_{3a}-SP MO-injected embryos.

Atp1a3b-deficient Embryos Phenocopy the Atp1a3a-deficient Embryos—We used a similar approach to assess the developmental role of the other *ATP1A3* ortholog, *Atp1a3b*. qRT-PCR analysis showed that the α_{3b}-SP-MO led to reductions in transcript levels of 22 and 66% when injected in amounts of 1.5 and 3 ng, respectively (Fig. 3*C*). Moreover, *Atp1a3b* KD embryos showed brain ventricle dilation phenotype similar to those produced by *Atp1a3a* KD embryos (Fig. 3, *A* and *B*). *Atp1a3b* KD caused severe brain ventricle dilation in 59% of the embryos, moderate dilation in 27% of the embryos, and no extraordinary ventricle dilation in 14% of the embryos, and std-MO-injected embryos appeared morphologically normal (Fig. 3, *A* and *D*). Co-injections of p53-MO ruled out the activation of p53-dependent apoptosis in *Atp1a3b* KD embryos (Fig. 3*A*). Upon co-injection with *in vitro* transcribed *Atp1a3b* mRNA, severe brain ventricle dilation was observed in 16% of the embryos, moderate dilation was observed in 24% of the embryos, and no ventricle dilation was observed in 61% of the embryos (Fig. 3*D*). Importantly, the brain ventricle dilation of *Atp1a3a* KD embryos was not rescued by co-injection of *Atp1a3b* mRNA, and conversely, *Atp1a3b* KD embryos were not rescued by co-injection of *Atp1a3a* mRNA (Fig. 3*E*).

The observation of similar phenotypes upon the use of two distinct MOs (Figs. 2*A* and 3*A*), and the fact that the nonsense-mediated mRNA decay of the targeted transcript by SP-MOs could be observed in a concentration-correlated manner (Figs. 2*C* and 3*C*), together verified the specificity of the MOs used in this study. In addition, our observations of consistent brain ventricle dilation phenotypes, even after p53-MO co-injection with each MO (Figs. 2*A* and 3*A*), and importantly, the significant rescue of the phenotypes by injection of the mRNA of the knocked down gene (Figs. 2*D* and 3*D*), further confirmed the specificity. It is important to note that full rescue of the brain ventricle dilation phenotype was not accomplished, most likely due to the limited stability of the injected exogenous mRNA in the cell.

Atp1a3a KD Leads to Depolarization of the Resting Membrane Potential of Rohon-Beard Neurons—RB cells are mechanosensory neurons localized in the dorsal spinal cord (35, 36) and are involved in response to touch, a behavior that involves both neuronal and muscular components. RB neurons are within the domain of *Atp1a3a* expression (Fig. 1*B*) and accessible due to their superficial localization. Combining the advantages of *Atp1a3a* being expressed in RB neurons and the accessibility of these cells, we measured electrophysiological changes at the cellular level in RB neurons of *Atp1a3a* KD embryos. The RMP of RB neurons was recorded using whole-cell patch clamp. The RMP of RB neurons in *Atp1a3a* KD embryos displaying severe brain ventricle dilation was significantly ($p < 0.01$) more depolarized (mean RMP: -46.6 ± 5.1 mV) as compared with the RMP from slight/no brain ventricle dilation-displaying *Atp1a3a* KD embryos (mean RMP: -70.4 ± 2.9 mV), which were comparable ($p > 0.05$) with the control groups, noninjected (mean RMP: -72.1 ± 1.7 mV), and std-MO-injected (mean RMP: -65.2 ± 3.1 mV) embryos (Fig. 4*A*). A schematic representation illustrates the consequence of the depolarized RMP in RB neurons in an *Atp1a3a* KD embryo (Fig. 4*B*).

Atp1a3a and Atp1a3b KD Embryos Differ in Their Mechanosensory Responses—The onset of *Atp1a3a* and *Atp1a3b* expression coincides with the ability of the embryo to respond to tactile stimulation at around 27 hpf (prim-6 stage), where a marked increase in the expression of both isoforms was detected (Fig. 1*A*). Considering that RB cells mediate touch sensitivity for the embryo, and that KD of *Atp1a3a* depolarized

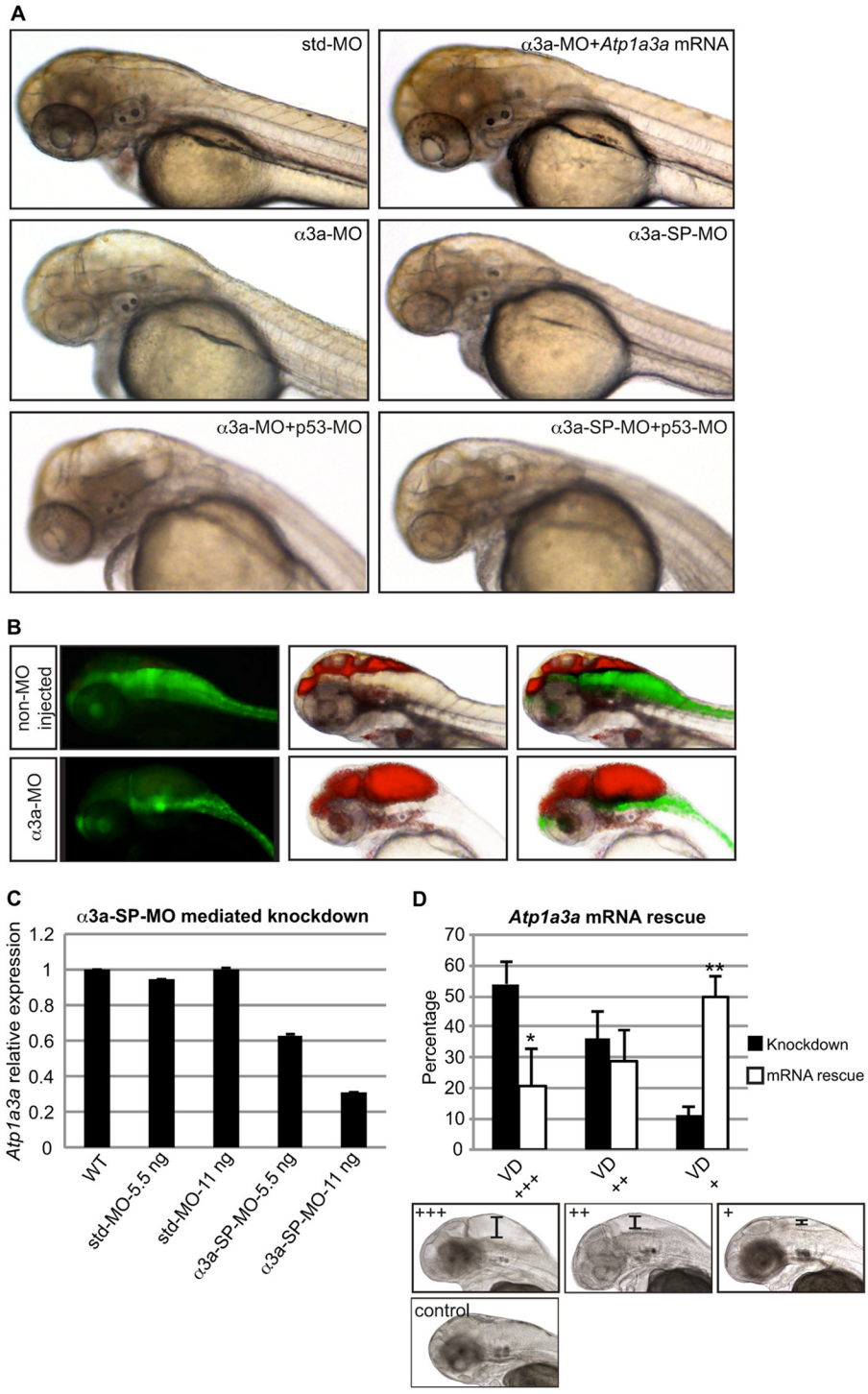

FIGURE 2. **Knockdown of *Atp1a3a* causes brain ventricle dilation.** *A*, significant brain ventricle dilation occurred in embryos upon *Atp1a3a* KD mediated by α_{3a}-MO or α_{3a}-SP-MO as compared with std-MO-injected control embryo. This phenotype was rescued by co-injection of *Atp1a3a* mRNA. p53-MO co-injections with any of the MOs did not rescue the brain ventricle dilation phenotype. *B*, brain ventricles of Tg(gfap:GFP) line, non-MO-injected and α_{3a}-MO-injected, were injected with rhodamine-conjugated dextran. Brain ventricles and the astrocytes are highlighted by *red* and *green fluorescence*, respectively. *C*, qRT-PCR tested efficiency of α_{3a}-SP-MO-mediated KD in terms of changes in the relative expression level of *Atp1a3a*. Data are presented as mean ± S.E. of triplicate measurements. Concentrations of MOs are indicated. *D*, mean percentages ± S.D. of the α_{3a}-SP-MO-injected embryos suffering from brain ventricle dilation of different severity, with (*white columns*, $n = 117$) and without (*black columns*, $n = 96$) *Atp1a3a* mRNA co-injection, are plotted. Embryos at the *lower panel* represent the extent of the brain ventricle dilation (*VD*) used as a criterion for grouping as severe (+++) (*scale bar*: ~235 μm), moderate (++) (*scale bar*: ~150 μm), and slight/no (+) (*scale bar*: ~65 μm). *, $p < 0.1$; **, $p < 0.01$.

the RB RMP, we tested for effects on tactile sensitivity. The RB-mediated touch response is assayed by applying tactile stimuli to the trunk of a motile embryo (37). Although both *Atp1a3a* KD and *Atp1a3b* KD embryos display abnormal spontaneous motility (data not shown), they are motile and suitable for assessment of tactile sensitivity.

At 60 hpf, the control embryos, noninjected (supplemental Movie 1) and std-MO-injected (supplemental Movie 2),

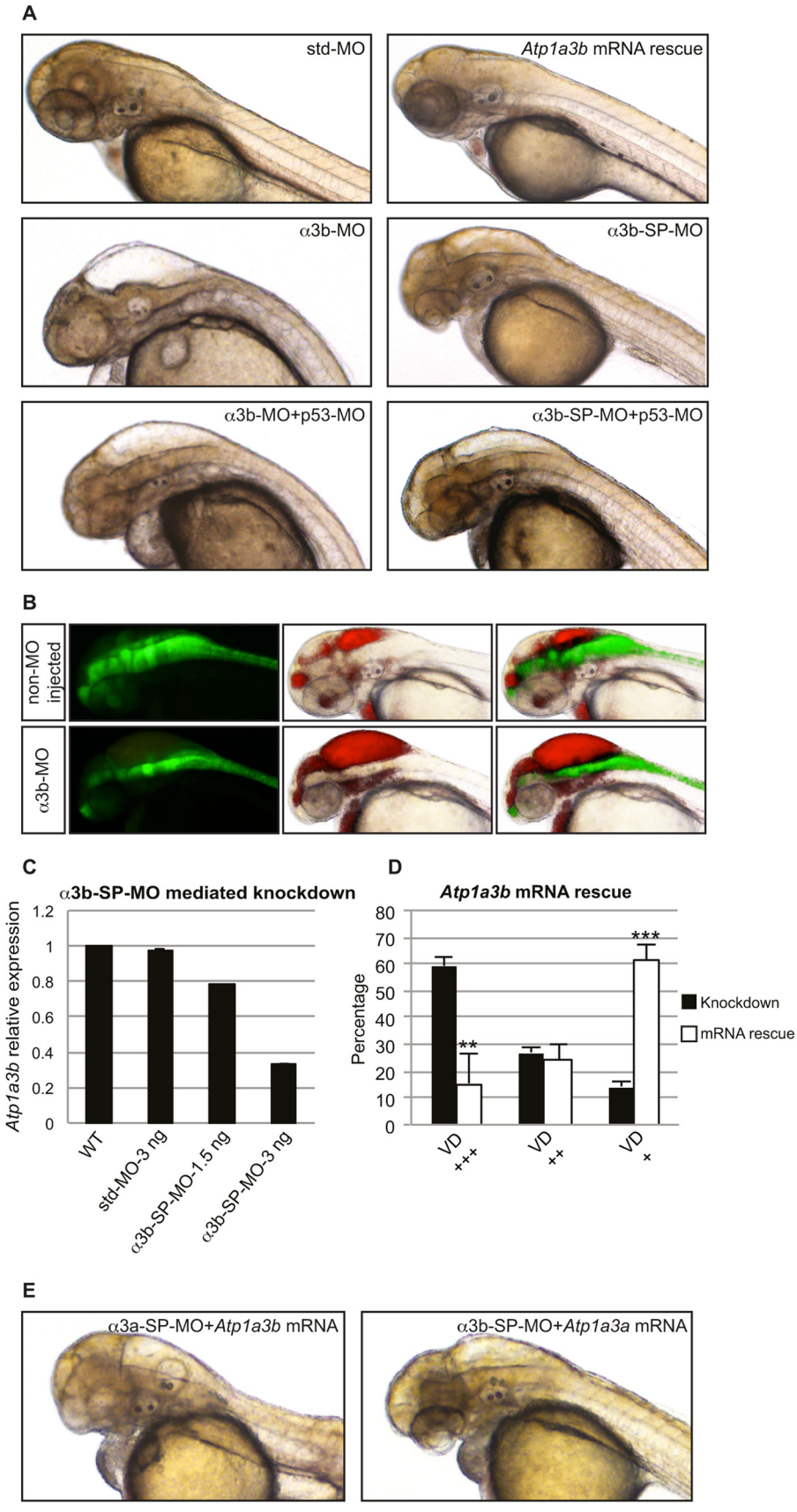
A
std-MO
Atp1a3b mRNA rescue
α3b-MO
α3b-SP-MO
α3b-MO+p53-MO
α3b-SP-MO+p53-MO
B
non-MO injected
α3b-MO
C
α3b-SP-MO mediated knockdown
Atp1a3b relative expression
1.2
1
0.8
0.6
0.4
0.2
0
WT
std-MO-3 ng
α3b-SP-MO-1.5 ng
α3b-SP-MO-3 ng
D
Atp1a3b mRNA rescue
Percentage
80
70
60
50
40
30
20
10
0
**
***
Knockdown
mRNA rescue
VD +++
VD ++
VD +
E
α3a-SP-MO+Atp1a3b mRNA
α3b-SP-MO+Atp1a3a mRNA

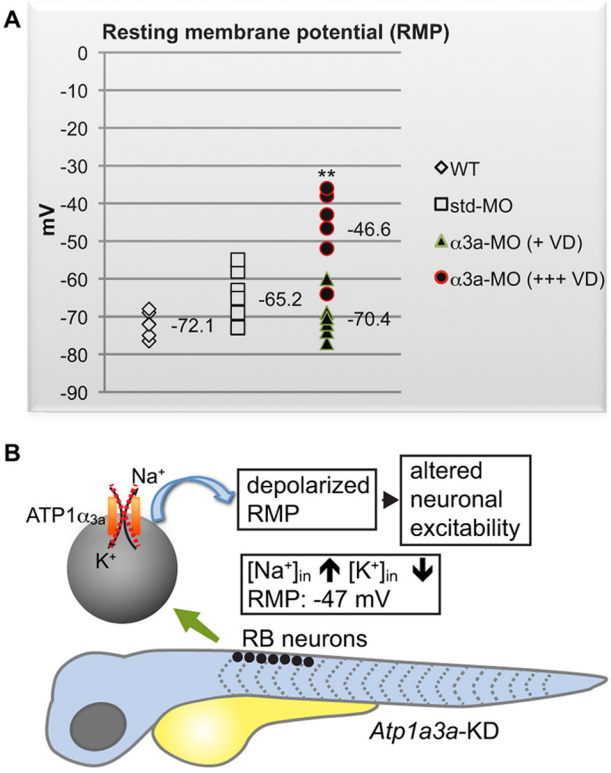

FIGURE 4. **RB neurons are more depolarized in *Atp1a3a* KD zebrafish displaying severe brain ventricle dilation.** *A*, RMP values of RB neurons from WT ($n = 5$), std-MO-injected ($n = 6$), and α_{3a}-MO-injected embryos ($n = 10$) are plotted. The α_{3a}-MO-injected embryos are divided into embryos displaying severe (+++) ($n = 5$) or slight/no (+) ($n = 5$) brain ventricle dilation (*VD*). The number of cells (*n*) recorded per group stems from at least three different animals. RMP data are presented as mean ± S.D. **, $p < 0.01$ between RMPs of α_{3a}-MO-injected embryos with severe ventricle dilation and control groups, WT, and std-MO-injected embryos. *B*, schematic representation summarizing the depolarization of the RMP in RB neurons in an *Atp1a3a* KD embryo. The scheme covers the time frame of 48–60 hpf. The *dashed cross* marks a malfunctioning $\alpha_{3a}Na^+/K^+$-ATPase.

responded by burst swimming as expected. *Atp1a3a* KD embryos (supplemental Movie 3) typically responded quickly to tactile stimulation but with a brief escape and circling movements that in one instance culminated in convulsion (supplemental Movie 3) (*top*). *Atp1a3b* KD also had a range of effects, some of which were similar to and others which were different from those produced by *Atp1a3a* KD (supplemental Movie 4). The most consistent difference was that *Atp1a3b* KD embryos responded with a delay in contrast to the quick response of *Atp1a3a* KD embryos. Similar to *Atp1a3a* KD embryos, *Atp1a3b* KD embryos also displayed brief distance recoils and, in one instance, convulsion (supplemental Movie 4) (*right*). Successive frame shots from touch response movies (supplemental Movies 1, 3, and 4) provide an overview of the embryonic movements and allow comparisons between the different experimental groups (Fig. 5). Taken together, the data indicate that *Atp1a3a* or *Atp1a3b* KD impair but do not prevent embryonic motility. In addition, the embryos retain the ability to respond to touch but, given the motility defects, it was difficult to assess whether there was any reduction in touch sensitivity, although this is indicated by RMP alterations in RB neurons in *Atp1a3a* KD and by delayed response in *Atp1a3b* KD embryos.

Atp1a3a KD Leads to Disorganization of the Brain but No Loss of Dopaminergic Neurons—A subset of dystonia subtypes responds to L-DOPA treatments that target DA neurons in the substantia nigra (38). However, RDP patients do not respond to L-DOPA treatment. To assess whether zebrafish α_3 isoforms differ in their association to DA neurons as compared with their mammalian counterparts, we questioned the presence of zebrafish α_3 isoforms in DA neurons. *Atp1a3a* co-localized with the DA neuron marker, TH (Fig. 6*A*), a marker previously used to identify DA neurons in zebrafish (39). Confocal images highlight the classical arrangement of TH-positive cells in the diencephalon, a region that shows widespread expression of *Atp1a3a* mRNA (Fig. 6*A*). The expression pattern of *Atp1a3b* (Fig. 1*C*) does not suggest co-expression of this isoform with DA neurons.

We then tested whether *Atp1a3a* KD affected DA neurons by comparing the distribution of *Th* transcripts in WT, α_{3a}-SP-MO-mediated *Atp1a3a* KD, and mRNA-rescued *Atp1a3a* KD embryos (Fig. 6*B*). Although there were some slight differences in the pattern and intensity of the *Th* mRNA signal (Fig. 6*B*), quantitative analysis showed no significant difference (Fig. 6*C*). The variations in *Th* expression profile observed in *Atp1a3a* KD zebrafish correlate with the extent of brain ventricle dilation and the consequent spatial reorganization in the brain, but not with loss of DA neurons. These results support the view that *Atp1a3a* KD does not lead to DA neuron degeneration.

Several Proteins Are Up/Down-regulated When Either Atp1a3a or Atp1a3b Is Knocked Down—To investigate the cellular protein networks that potentially involve α_3Na^+/K^+-ATPases, we carried out proteomics analyses. Candidate proteins affected in *Atp1a3a* or *Atp1a3b* KD embryos were identified using iTRAQ and listed together with their known tissue associations (supplemental Table S1). Interestingly, several candidates are of relevance to Na^+/K^+-ATPase and *Atp1a3a* or *Atp1a3b* KD phenotypes (Table 1), but only selected candidates are discussed below. It is interesting to note that cytoskeletal and muscle-associated proteins appear to be regulated by both α_3 isoforms. In contrast, the level of ion-binding proteins and proteins involved in phosphate metabolism appear to depend on the α_{3b} isoform.

We performed qRT-PCR to verify selected proteomic candidates as antibodies toward all of these zebrafish proteins were

FIGURE 3. **Knockdown of *Atp1a3b* phenocopies *Atp1a3a* knockdown.** *A*, brain ventricle dilation was observed in embryos upon *Atp1a3b* KD mediated by α_{3b}-MO- or α_{3b}-SP-MO-injected embryo as compared with the std-MO-injected control embryo. This phenotype was rescued by co-injection of *Atp1a3b* mRNA. p53-MO co-injections with any of the MOs did not rescue the brain ventricle dilation phenotype. *B*, brain ventricles of Tg(gfap:GFP) line, non-MO-injected and α_{3b}-MO-injected, were injected with rhodamine-conjugated dextran. Brain ventricles and the astrocytes are highlighted by *red* and *green fluorescence*, respectively. *C*, α_{3b}-SP-MO-mediated KD efficiency was tested by qRT-PCR in terms of changes in the relative expression level of *Atp1a3b*. Data are presented as mean ± S.E. of triplicate measurements. Concentrations of MOs are indicated. *D*, mean percentages ± S.D. of the α_{3b}-SP-MO-injected embryos suffering from brain ventricle dilation (*VD*) of different severity, with (*white columns*, $n = 148$) and without (*black columns*, $n = 88$) *Atp1a3a* mRNA co-injection, are plotted. The degree of brain ventricle dilation is as follows: +, slight/no; ++, moderate; +++, severe. **, $p < 0.01$; ***, $p < 0.001$. *E*, *Atp1a3a* mRNA did not rescue α_{3b}-SP-MO-injected embryos; similarly, *Atp1a3b* mRNA did not rescue α_{3a}-SP-MO-injected embryos from brain ventricle dilation.

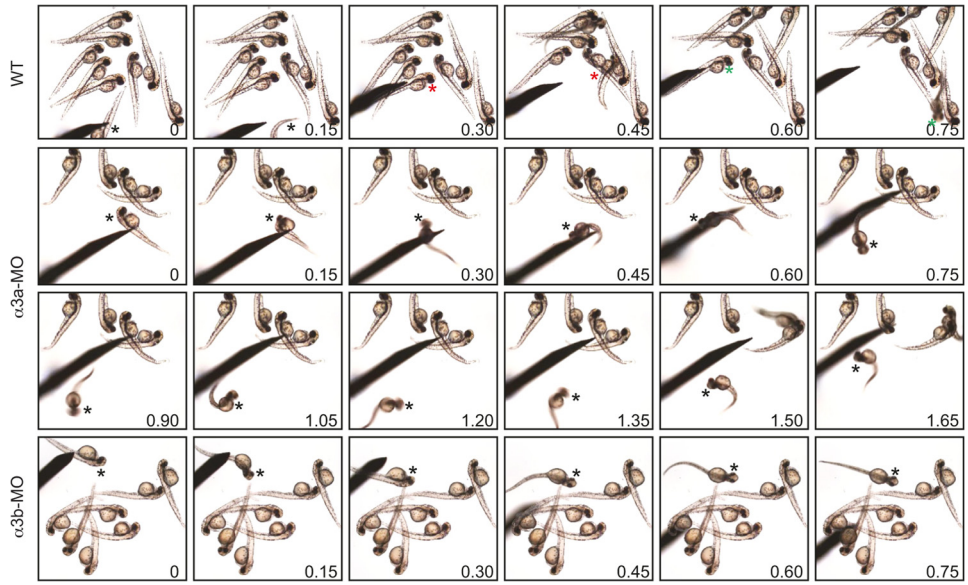

FIGURE 5. **Atp1a3a and *Atp1a3b* KD embryos respond to touch but have abnormal motility.** Successive frame shots from touch response assay display three representative WT embryos with burst swimming response (*top panel*, supplemental Movie 1), a representative α_{3a}-MO-injected embryo that kept swirling around itself (*middle panels*, supplemental Movie 3), and a α_{3b}-MO-injected embryo that responded as a short distance recoil (*bottom panel*, supplemental Movie 4). Touch-stimulated embryos are marked with a *color-coded asterisk*, and the frame shot times are merged on images in seconds.

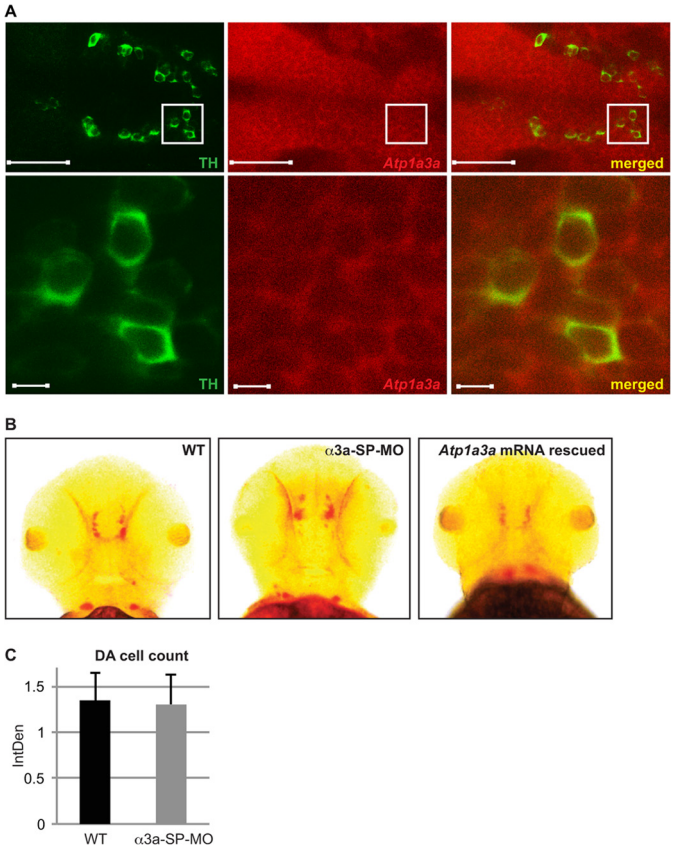

FIGURE 6. **Atp1a3a mRNA is present in DA neurons, but no loss of DA neuron was observed in *Atp1a3a* KD embryos.** *A*, TH-positive DA neurons (*green fluorescence*) and *Atp1a3a* mRNA expression (*red fluorescence*) in the zebrafish brain are imaged along the dorsoventral axis (anterior to the *left*; posterior to the *right*). *Scale bars* represent 50 μm. Areas marked by *squares* are shown in the *lower panel* at higher magnification (*scale bars* represent 5 μm). *B*, *Th* mRNA expression analyzed by *in situ* hybridization in WT, α_{3a}-SP-MO-injected, and *Atp1a3a* mRNA-rescued embryos. *C*, total staining of *Th* mRNA in WT ($n = 10$) and α_{3a}-SP-MO-injected embryos ($n = 10$) was quantified using ImageJ, and mean values of integrated densities (*IntDen*) are plotted with standard deviations.

not available. We found that these transcripts were also down-regulated in *Atp1a3a* or *Atp1a3b* KD embryos, supporting the proteomics data at the transcript level (Fig. 7, *A* and *B*).

DISCUSSION

In this study, we analyzed zebrafish α_3Na$^+$/K$^+$-ATPases to gain insight on specific functions of this particular ion pump and how we might use this model to elucidate the functions of the Na$^+$/K$^+$-ATPase in brain development. The Na$^+$/K$^+$-ATPase has a well known role as a modulator of membrane potential in neurons and is essential for generating an action potential. Consistent with the mammalian ATP1α_3 expression, both *ATP1A3* zebrafish orthologs are expressed primarily in the brain. Interestingly, the expression of the *Atp1a3a* mRNA is widely distributed in the brain, in contrast to a more restricted expression of the *Atp1a3b* mRNA, in line with the expression data available at The Zebrafish Model Organism Database. The *Atp1a3a* transcript was also abundant in the spinal cord and, to a lesser extent, in the heart. The latter observation is consistent with previous studies demonstrating ATP1α_3 expression in the neonatal, but not adult, rat heart (40, 41).

Despite the distinct expression profiles of *Atp1a3a* and *Atp1a3b* transcripts, both *Atp1a3a* and *Atp1a3b* deficiencies cause brain ventricle dilation, rather than cellular swelling, indicating an altered fluid and electrolyte balance. Possibly, the subset of ventral CNS regions that express both *Atp1a3a* and *Atp1a3b* involves a pathological pathway that results in this phenotype A functional Na$^+$/K$^+$-ATPase, in a complex with aquaporins and glutamate transporters, and is important for maintaining water and ion balance in the brain (42). Interestingly, Na$^+$/K$^+$-ATPase, in particular *Atp1a1*, was previously demonstrated to be required for the zebrafish brain ventricle development (19, 43). However, our data suggest that *Atp1a3a* and *Atp1a3b* KD do not inhibit ventricle inflation, but the consequent phenotype is connected to dilated ventricles as a result

TABLE 1

List of regulated proteins selected from proteomics assay

Proteins relevant for the *Atp1a3a* and *Atp1a3b* KD phenotypes were selected from supplemental Table S1. Proteins were detected by iTRAQ LC-MS/MS. Database accession numbers, gene identity, relative-fold change, and tissue associations are given. The *Atp1a3* KD/control protein expression ratio indicates up-regulation when it is equal/above 2 and down-regulation when it is equal/below 0.5.

Accession number	Description	Gene	*Atp1a3a* KD/control (116/114)	Tissue association
39645432	Krt5 protein	*Krt5*	0.5	Epidermis, eye
44890667	Krt4 protein	*Krt4*	0.5	Epidermis
158253775	Zgc:165344 protein	*Zgc:165344*	0.5	Myotome
Accession number	**Description**	**Gene**	***Atp1a3b* KD/control (117/114)**	**Tissue association**
45387573	Parvalbumin isoform 1d	*Pvalb1*	0.2	Myotome
123916361	RecName: Full = betaine-homocysteine S-methyltransferase 1	*Bhmt*	0.3	All
50512294	Myosin, heavy polypeptide 2, fast muscle-specific	*Mhyz2*	0.3	Muscle
41053595	Nucleoside diphosphate kinase B	*Ndpkz2*	0.3	Brain, eye, muscle
41056123	Phosphoglycerate mutase 2	*Pgam2*	0.4	Heart, myotome
68366260	Predicted: glutathione *S*- transferase θ 1a	*Gstt1a*	0.4	Retina, head mesenchyme
33636707	Parvalbumin 9	*Pvalb9*	0.4	
157787181	Muscle creatine kinase b	*Ckmb*	0.4	Eye, heart, myotome
123229625	Creatine kinase, muscle	*Ckma*	0.5	Eye, heart, myotome
51571925	Adenylate kinase isoenzyme 1	*Zgc:91930*	0.5	Myotome, somite
157888726	Glucose phosphate isomerase b	*Gpib*	0.5	Eye, heart, myotome
157743330	Guanidinoacetate *N*- methyltransferase	*Gamt*	0.5	Brain
167234796	si:dkeyp-113d7.4	si:dkeyp-*113d7.4*	0.5	Intermediate filament

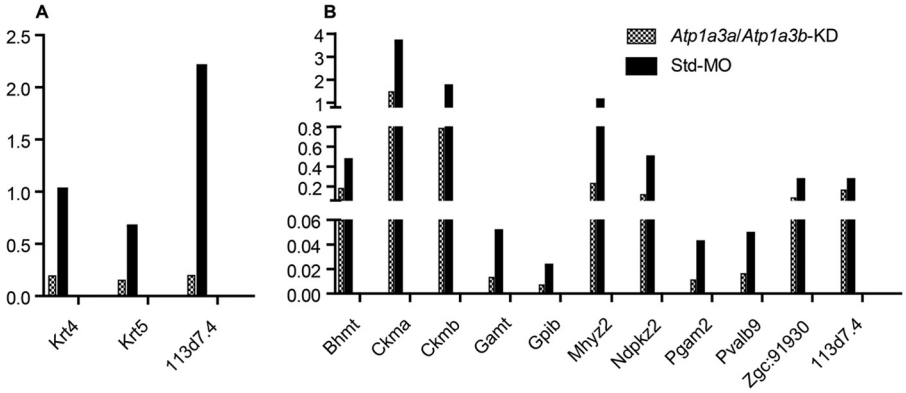

FIGURE 7. **Relative mRNA expressions of some of the regulated proteins detected in proteomics assay.** *A* and *B*, mRNA expressions of selected proteins regulated by α_{3a}-MO-mediated *Atp1a3a* KD (*A*) or α_{3b}-MO-mediated *Atp1a3b* KD (*B*) were quantified by qRT-PCR and normalized to *Actb2* expression in embryos at 60 hpf. Data are presented as mean ± S.E. of triplicate measurements.

of cerebrospinal fluid (CSF) accumulation. An increase or a decrease in the CSF volume can be pathological throughout life (44), and the Na^+/K^+-ATPase may serve to sense the ventricular volume in a homeostatic role. Consequently, even a slight disruption of Na^+/K^+-ATPase subunits could lead to significant changes in CSF volume. Overall, these data indicate a role of α_3Na^+/K^+-ATPase in brain ventricle volume maintenance through its ion pump function. CSF composition is vital to brain health. The protein function of the α_3Na^+/K^+-ATPase in neurons is likely connected to the extrusion of Na^+ to the extracellular space coupled to the uptake of K^+ into the intracellular cytoplasm. This exchange of Na^+/K^+ ions generates an electrochemical gradient, which, in turn, facilitates ion transport, for example of Cl^-, HCO_3^-, and H_2O, required to regulate CSF volume (45). Interestingly, a recent study showed that increases in aquaporin-1 (AQP1) and cation chloride transporters (Na^+-K^+-$2Cl^-$ cotransporter 1 (NKCC1)) expression under hyposmotic stress may be one of the molecular mechanisms underlying the pathophysiology of acute hyponatremia by increasing water transport across the blood-CSF barrier (46).

It is very interesting that the distinctively expressed α_3 isoforms both result in brain ventricle dilation when knocked down, and moreover, that they are not able to cross rescue. This indicates that at some level, the ion pump function must be the major mechanism behind our observations despite the different proteomic changes when knocked down. Furthermore, we do not know at this stage to what extent other Na^+/K^+-ATPase isoforms are active in the cells expressing these α_3 isoforms.

Modeling human diseases in other organisms requires complex analysis. Of particular relevance for this study is the fact that the water environment hosting zebrafish differs from other environments and thus requires other mechanisms for ion homeostasis to maintain osmolarity. However, we believe that it is not so extraordinary to observe a brain ventricle dilation phenotype in the *Atp1a3* KD zebrafish, although this is not a manifestation observed in RDP patients harboring mutations in the *ATP1A3* gene (47). Thus, we cannot rule out that the brain ventricle dilation is specific to zebrafish despite the conserved functions of the Na^+/K^+-ATPase. The CSF fills the ventricle of the brain, and the composition of the CSF influences neu-

ronal activity and serves as a drainage pathway for the brain. The latter function might be significantly different in water-living animals. In summary, it appears that the α_3Na$^+$/K$^+$-ATPase is a novel regulator of brain ventricle volume, at least in zebrafish.

Minor changes in ion composition in the extracellular and intracellular compartments of the brain can significantly affect neuronal function, which relies on precise ion gradients across their plasma membranes to trigger changes in membrane potentials underlying action potential generation and propagation. Therefore, ion and water transport in the brain are tightly regulated (48). The most studied role of the α_3 isoform is its neuronal function, and failure of the Na$^+$/K$^+$-ATPase to maintain Na$^+$ and K$^+$ gradients leads to a decrease in both the RMP and the action potential and to altered neuronal excitability in several different neurons, such as rat hippocampus dentate interneurons, and pyramidal and Purkinje neurons (49). Consistent with this, we found that RB neurons had depolarized RMPs when *Atp1a3a* was knocked down. This result is important and additionally serves to strongly support the specificity of the *Atp1a3* KD phenotypes. The change in the electrophysiological state of the RB neurons is thus predicted to alter the neuronal excitability, although future *in vivo* measurements of excitability are required to address this. Our data strongly support a neuronal function for α_3 isoforms in zebrafish. We believe that it is important to keep in mind that the RMP recording is performed in RB neurons and the ventricle dilation is observed in the brain. We do not yet know the contributions from other Na$^+$/K$^+$-ATPase isoforms in these cell populations, and this could certainly explain why we could not demonstrate an altered RMP in the slight (if any) brain ventricle dilation-displaying embryos.

The production of any touch response in zebrafish can be divided into several steps from sensory perception to muscle activation. The mechanosensory neurons, in this case RB neurons, sense touch stimuli. Once triggered by sensory input, interneuronal networks located in the hindbrain and spinal cord produce the appropriate motor rhythm (50). Depolarization in RB neurons indicated abnormality in the sensory component of this type of behavior, although further experiments are needed to distinguish all the contributors of this phenotype. It is intriguing because the motor deficits observed in $\alpha_3^{+/-}$KO mice were shown to have neuronal origin (16). Furthermore, inefficient central sensory-motor processing has been suggested to be a possible causative mechanism for dystonia, and numerous clinical phenomena suggest the primary involvement of the somatosensory system in this disorder (51, 52).

Intriguingly, a recent study reported Na$^+$/K$^+$-ATPase as an important player in locomotor behavior of frog tadpoles (53) and of *Drosophila* larvae (54). Also, in spinal network of neonatal rats, blocking of Na$^+$/K$^+$ pump activity disrupts rhythmic bursting of lumbar motor neurons (55, 56). Moreover, the pump function of Na$^+$/K$^+$-ATPase was recognized as a mechanism to gate sensory information entering the spinal cord, where it alters neuronal excitability (57). By a similar mechanism, the changes in neuronal excitability might account for the impaired spontaneous motility of the *Atp1a3a* and *Atp1a3b* KD embryos.

Treatment of RDP patients with L-DOPA has no effect, and the DA reuptake sites appear normal in such patients (58). Although studies in mouse brain did not detect the α_3 isoform in DA neurons of substantia nigra (8), it is interesting that another subunit, the β subunit, ATP1β_1, is down-regulated in DA neurons of patients with Parkinson disease (59). We detected *Atp1a3a* expression in zebrafish TH-positive cells. In line with this, a recent study identified *Atp1a3a* as a target of a cardiac glycoside (a Na$^+$/K$^+$-ATPase inhibitor; Neriifolin), which impairs DA neuronal survival (60). However, our results show that *Atp1a3a* KD does not result in loss of DA neurons in zebrafish, although we did observe reorganization in the DA neuron distribution profile. The latter is most likely caused by spatial restrictions due to the brain ventricle dilation, also noted in the Tg(gfap:GFP) *Atp1a3a* and *Atp1a3b* KD embryos.

We also identified novel proteomic changes associated with the α_3 isoform deficiencies. This is in fact the first time a proteomic approach has been used to identify proteins up- or down-regulated in ATP1α_3-deficient cells. Interestingly, a recent study explored proteomic changes in ATP1α_2-deficient zebrafish (18), and some of the regulated proteins, *e.g.* parvalbumin and muscle creatine kinase, published in that study were also detected as regulated in *Atp1a3b*-deficient embryos, indicating that the link between these proteins and the Na$^+$/K$^+$-ATPase is most likely dependent on the Na$^+$/K$^+$-ATPase pump function, rather than an isoform-specific association. Hence, although preliminary, it provides an important initiative to be further assessed. To functionally address these candidate proteins in relation to the obtained *Atp1a3a* and *Atp1a3b* KD zebrafish and other animal models will be a future direction of this project.

Of particular interest is the down-regulation of parvalbumin detected in our proteomics assay of the *Atp1a3a* KD embryos. Parvalbumin is expressed preferentially in a subpopulation of GABAergic neurons in mice, overlapping with the α_3Na$^+$/K$^+$-ATPase expression (8, 61, 62). Parvalbumin modulates short term synaptic plasticity (63) and thus compliments the signaling role of the α_3Na$^+$/K$^+$-ATPase in synaptic plasticity and in dendritic growth in cortical neurons (64). Neuronal associations of α_3Na$^+$/K$^+$-ATPase are further supported by the down-regulation of guanidinoacetate methyltransferase (GAMT). The guanidinoacetate is the principal metabolite accumulating in guanidinoacetate methyltransferase deficiency, which significantly inhibits Na$^+$/K$^+$-ATPase activity (65). It was proposed that such inhibition may be one of the mechanisms involved in the neuronal dysfunction observed in patients suffering from guanidinoacetate methyltransferase deficiency, which shows symptoms comparable with RDP: *e.g.* muscle weakness, epilepsy, and seizures (65, 66).

Although it is clear that zebrafish embryos will not develop a full range of complex, human-like disorders, they can be used to study certain biological markers (endophenotypes) of these disorders. Indeed, several features of zebrafish α_3 isoforms are comparable with the mammalian counterparts. This study comprehensively examined the spatial distribution of the zebrafish *ATP1A3* orthologs and is the first study to show that the two distinctively expressed α_3 isoforms caused enlarged brain ventricle when gene functions were diminished. This was

accompanied with abrupt embryonic motility, most likely linked to depolarized RMP, as shown for the spinal RB neurons, and this, combined with our proteomic data, highly promotes zebrafish as a relevant model to further assess α_3Na^+/K^+-ATPase in brain development, neuronal excitability, and thus neuronal functions.

Acknowledgments—We thank C. Knoeckel and R. Moreno, Department of Physiology and Biophysics, University of Colorado, Denver, for the assistance in whole-cell patch clamp electrophysiology recordings and J. R. Nyengaard, Aarhus University, Department of Biomedicine for the help on sectioning.

REFERENCES

1. Blanco, G. (2005) Na,K-ATPase subunit heterogeneity as a mechanism for tissue-specific ion regulation. *Semin. Nephrol.* **25,** 292–303
2. Kaplan, J. H. (2002) Biochemistry of Na,K-ATPase. *Annu. Rev. Biochem.* **71,** 511–535
3. Lingrel, J., Moseley, A., Dostanic, I., Cougnon, M., He, S., James, P., Woo, A., O'Connor, K., and Neumann, J. (2003) Functional roles of the α isoforms of the Na,K-ATPase. *Ann. N.Y. Acad. Sci.* **986,** 354–359
4. Lingrel, J. B., and Kuntzweiler, T. (1994) Na^+,K^+-ATPase. *J. Biol. Chem.* **269,** 19659–19662
5. McGrail, K. M., Phillips, J. M., and Sweadner, K. J. (1991) Immunofluorescent localization of three Na,K-ATPase isozymes in the rat central nervous system: both neurons and glia can express more than one Na,K-ATPase. *J. Neurosci.* **11,** 381–391
6. Shull, G. E., Greeb, J., and Lingrel, J. B. (1986) Molecular cloning of three distinct forms of the Na^+,K^+-ATPase α-subunit from rat brain. *Biochemistry* **25,** 8125–8132
7. Schneider, J. W., Mercer, R. W., Caplan, M., Emanuel, J. R., Sweadner, K. J., Benz, E. J., Jr., and Levenson, R. (1985) Molecular cloning of rat brain Na,K-ATPase α-subunit cDNA. *Proc. Natl. Acad. Sci. U.S.A.* **82,** 6357–6361
8. Bøttger, P., Tracz, Z., Heuck, A., Nissen, P., Romero-Ramos, M., and Lykke-Hartmann, K. (2011) Distribution of Na/K-ATPase α3 isoform, a sodium-potassium P-type pump associated with rapid-onset of dystonia parkinsonism (RDP) in the adult mouse brain. *J Comp. Neurol.* **519,** 376–404
9. Brashear, A., DeLeon, D., Bressman, S. B., Thyagarajan, D., Farlow, M. R., and Dobyns, W. B. (1997) Rapid-onset dystonia-parkinsonism in a second family. *Neurology* **48,** 1066–1069
10. de Carvalho Aguiar, P., Sweadner, K. J., Penniston, J. T., Zaremba, J., Liu, L., Caton, M., Linazasoro, G., Borg, M., Tijssen, M. A., Bressman, S. B., Dobyns, W. B., Brashear, A., and Ozelius, L. J. (2004) Mutations in the Na^+/K^+-ATPase α3 gene *ATP1A3* are associated with rapid-onset dystonia parkinsonism. *Neuron* **43,** 169–175
11. Brashear, A., Dobyns, W. B., de Carvalho Aguiar, P., Borg, M., Frijns, C. J., Gollamudi, S., Green, A., Guimaraes, J., Haake, B. C., Klein, C., Linazasoro, G., Münchau, A., Raymond, D., Riley, D., Saunders-Pullman, R., Tijssen, M. A., Webb, D., Zaremba, J., Bressman, S. B., and Ozelius, L. J. (2007) The phenotypic spectrum of rapid-onset dystonia-parkinsonism (RDP) and mutations in the *ATP1A3* gene. *Brain* **130,** 828–835
12. Desfrere, L., Karlsson, M., Hiyoshi, H., Malmersjö, S., Nanou, E., Estrada, M., Miyakawa, A., Lagercrantz, H., El Manira, A., Lal, M., and Uhlén, P. (2009) Na,K-ATPase signal transduction triggers CREB activation and dendritic growth. *Proc. Natl. Acad. Sci. U.S.A.* **106,** 2212–2217
13. Dobretsov, M., Hastings, S. L., Sims, T. J., Stimers, J. R., and Romanovsky, D. (2003) Stretch receptor-associated expression of α3 isoform of the Na^+, K^+-ATPase in rat peripheral nervous system. *Neuroscience* **116,** 1069–1080
14. Moseley, A. E., Williams, M. T., Schaefer, T. L., Bohanan, C. S., Neumann, J. C., Behbehani, M. M., Vorhees, C. V., and Lingrel, J. B. (2007) Deficiency in Na,K-ATPase α isoform genes alters spatial learning, motor activity, and anxiety in mice. *J. Neurosci.* **27,** 616–626
15. Clapcote, S. J., Duffy, S., Xie, G., Kirshenbaum, G., Bechard, A. R., Rodacker Schack, V., Petersen, J., Sinai, L., Saab, B. J., Lerch, J. P., Minassian, B. A., Ackerley, C. A., Sled, J. G., Cortez, M. A., Henderson, J. T., Vilsen, B., and Roder, J. C. (2009) Mutation I810N in the α3 isoform of Na^+,K^+-ATPase causes impairments in the sodium pump and hyperexcitability in the CNS. *Proc. Natl. Acad. Sci. U.S.A.* **106,** 14085–14090
16. DeAndrade, M. P., Yokoi, F., van Groen, T., Lingrel, J. B., and Li, Y. (2011) Characterization of *Atp1a3* mutant mice as a model of rapid-onset dystonia with parkinsonism. *Behav. Brain Res.* **216,** 659–665
17. Kirshenbaum, G. S., Clapcote, S. J., Duffy, S., Burgess, C. R., Petersen, J., Jarowek, K. J., Yücel, Y. H., Cortez, M. A., Snead, O. C., 3rd, Vilsen, B., Peever, J. H., Ralph, M. R., and Roder, J. C. (2011) Mania-like behavior induced by genetic dysfunction of the neuron-specific Na^+,K^+-ATPase α3 sodium pump. *Proc. Natl. Acad. Sci. U.S.A.* **108,** 18144–18149
18. Doganli, C., Kjaer-Sorensen, K., Knoeckel, C., Beck, H. C., Nyengaard, J. R., Honoré, B., Nissen, P., Ribera, A., Oxvig, C., and Lykke-Hartmann, K. (2012) The α2Na^+/K^+-ATPase is critical for skeletal and heart muscle function in zebrafish. *J. Cell Sci.*, in press
19. Chang, J. T., Lowery, L. A., and Sive, H. (2012) Multiple roles for the Na,K-ATPase subunits, Atp1a1 and Fxyd1, during brain ventricle development. *Dev. Biol.* **368,** 312–322
20. Barut, B. A., and Zon, L. I. (2000) Realizing the potential of zebrafish as a model for human disease. *Physiol Genomics.* **2,** 49–51
21. Lieschke, G. J., and Currie, P. D. (2007) Animal models of human disease: zebrafish swim into view. *Nat Rev Genet.* **8,** 353–367
22. Friedrich, R. W., Jacobson, G. A., and Zhu, P. (2010) Circuit neuroscience in zebrafish. *Curr. Biol.* **20,** R371–R381
23. Rajarao, S. J., Canfield, V. A., Mohideen, M. A., Yan, Y. L., Postlethwait, J. H., Cheng, K. C., and Levenson, R. (2001) The repertoire of Na,K-ATPase α and β subunit genes expressed in the zebrafish, *Danio rerio*. *Genome Res.* **11,** 1211–1220
24. Westerfield, D. (1995) *The Zebrafish Book: A Guide for the Laboratory Use of Zebrafish (Brachydanio rerio)*, pp. 787–801, University of Oregon Press, Eugene, OR
25. Kimmel, C. B., Ballard, W. W., Kimmel, S. R., Ullmann, B., and Schilling, T. F. (1995) Stages of embryonic development of the zebrafish. *Dev. Dyn.* **203,** 253–310
26. Doğanlı, C., Kjærgaard, T., Olsen, A., Oxvig, C., Füchtbauer, E. M., and Lykke-Hartmann, K. (2010) Early developmental expression of *Mus musculus* zinc finger RNA-binding protein compared to orthologs in *Caenorhabditis elegans* and *Danio rerio* and subcellular localization of *Mus musculus* and *Caenorhabditis elegans* zinc finger RNA-binding protein in 2-cell *Mus musculus* embryos. *DNA Cell Biol.* **29,** 713–727
27. Marshall, O. J. (2004) PerlPrimer: cross-platform, graphical primer design for standard, bisulphite, and real-time PCR. *Bioinformatics* **20,** 2471–2472
28. Chomczynski, P., and Mackey, K. (1995) Short technical reports. Modification of the TRI reagent procedure for isolation of RNA from polysaccharide- and proteoglycan-rich sources. *BioTechniques* **19,** 942–945
29. Thisse, C., and Thisse, B. (2008) High-resolution *in situ* hybridization to whole-mount zebrafish embryos. *Nat. Protoc.* **3,** 59–69
30. Gutzman, J. H., and Sive, H. (2009) Zebrafish brain ventricle injection. *J. Vis. Exp.* **26,** pii: 1218
31. Schulte-Merker, S., Ho, R. K., Herrmann, B. G., and Nüsslein-Volhard, C. (1992) The protein product of the zebrafish homologue of the mouse T gene is expressed in nuclei of the germ ring and the notochord of the early embryo. *Development* **116,** 1021–1032
32. Moreno, R. L., and Ribera, A. B. (2009) Zebrafish motor neuron subtypes differ electrically prior to axonal outgrowth. *J. Neurophysiol.* **102,** 2477–2484
33. Beck, H. C., Petersen, J., Felthaus, O., Schmalz, G., and Morsczeck, C. (2011) Comparison of neurosphere-like cell clusters derived from dental follicle precursor cells and retinal Muller cells. *Neurochem. Res.* **36,** 2002–2007
34. Robu, M. E., Larson, J. D., Nasevicius, A., Beiraghi, S., Brenner, C., Farber, S. A., and Ekker, S. C. (2007) p53 activation by knockdown technologies. *PLoS Genet.* **3,** e78
35. Clarke, J. D., Hayes, B. P., Hunt, S. P., and Roberts, A. (1984) Sensory physiology, anatomy and immunohistochemistry of Rohon-Beard neu-

rones in embryos of *Xenopus laevis*. *J. Physiol.* **348,** 511–525
36. Ribera, A. B., and Nüsslein-Volhard, C. (1998) Zebrafish touch-insensitive mutants reveal an essential role for the developmental regulation of sodium current. *J. Neurosci.* **18,** 9181–9191
37. Pineda, R. H., Heiser, R. A., and Ribera, A. B. (2005) Developmental, molecular, and genetic dissection of I_{Na} *in vivo* in embryonic zebrafish sensory neurons. *J. Neurophysiol.* **93,** 3582–3593
38. Nemeth, A. H. (1993) Dystonia Overview. in *GeneReviews* (Pagon, R. A., Bird, T. D., Dolan, C. R., Stephens, K., and Adam, M. P., eds), University of Washington, Seattle, WA
39. Flinn, L., Mortiboys, H., Volkmann, K., Köster, R. W., Ingham, P. W., and Bandmann, O. (2009) Complex I deficiency and dopaminergic neuronal cell loss in parkin-deficient zebrafish (*Danio rerio*). *Brain* **132,** 1613–1623
40. Shyjan, A. W., and Levenson, R. (1989) Antisera specific for the α1, α2, α3, and β subunits of the Na,K-ATPase: differential expression of α and β subunits in rat tissue membranes. *Biochemistry* **28,** 4531–4535
41. Sweadner, K. J., and Farshi, S. K. (1987) Rat cardiac ventricle has two Na^+,K^+-ATPases with different affinities for ouabain: developmental changes in immunologically different catalytic subunits. *Proc. Natl. Acad. Sci. U.S.A.* **84,** 8404–8407
42. Illarionova, N. B., Gunnarson, E., Li, Y., Brismar, H., Bondar, A., Zelenin, S., and Aperia, A. (2010) Functional and molecular interactions between aquaporins and Na,K-ATPase. *Neuroscience* **168,** 915–925
43. Lowery, L. A., and Sive, H. (2005) Initial formation of zebrafish brain ventricles occurs independently of circulation and requires the *nagie oko* and *snakehead*/*atp1a1a.1* gene products. *Development* **132,** 2057–2067
44. Lowery, L. A., and Sive, H. (2009) Totally tubular: the mystery behind function and origin of the brain ventricular system. *BioEssays* **31,** 446–458
45. Johanson, C. E., Duncan, J. A., 3rd, Klinge, P. M., Brinker, T., Stopa, E. G., and Silverberg, G. D. (2008) Multiplicity of cerebrospinal fluid functions: New challenges in health and disease. *Cerebrospinal Fluid Res.* **5,** 10
46. Kim, J., and Jung, Y. (2012) Increased aquaporin-1 and Na^+-K^+-$2Cl^-$ cotransporter 1 expression in choroid plexus leads to blood-cerebrospinal fluid barrier disruption and necrosis of hippocampal CA1 cells in acute rat models of hyponatremia. *J. Neurosci. Res.* **90,** 1437–1444
47. Bøttger, P., Doğanlı, C., and Lykke-Hartmann, K. (2012) Migraine- and dystonia-related disease-mutations of Na^+/K^+-ATPases: Relevance of behavioral studies in mice to disease symptoms and neurological manifestations in humans. *Neurosci. Biobehav. Rev.* **36,** 855–871
48. Kahle, K. T., Simard, J. M., Staley, K. J., Nahed, B. V., Jones, P. S., and Sun, D. (2009) Molecular mechanisms of ischemic cerebral edema: role of electroneutral ion transport. *Physiology* **24,** 257–265
49. Dobretsov, M., and Stimers, J. R. (2005) Neuronal function and α3 isoform of the Na/K-ATPase. *Front. Biosci.* **10,** 2373–2396
50. Fetcho, J. R. (1992) The spinal motor system in early vertebrates and some of its evolutionary changes. *Brain Behav. Evol.* **40,** 82–97
51. Hallett, M. (1995) Is dystonia a sensory disorder? *Ann. Neurol.* **38,** 139–140
52. Fiorio, M., Gambarin, M., Valente, E. M., Liberini, P., Loi, M., Cossu, G., Moretto, G., Bhatia, K. P., Defazio, G., Aglioti, S. M., Fiaschi, A., and Tinazzi, M. (2007) Defective temporal processing of sensory stimuli in DYT1 mutation carriers: a new endophenotype of dystonia? *Brain* **130,** 134–142
53. Zhang, H. Y., and Sillar, K. T. (2012) Short-term memory of motor network performance via activity-dependent potentiation of Na^+/K^+ pump function. *Curr. Biol.* **22,** 526–531
54. Pulver, S. R., and Griffith, L. C. (2010) Spike integration and cellular memory in a rhythmic network from Na^+/K^+ pump current dynamics. *Nat. Neurosci.* **13,** 53–59
55. Rozzo, A., Ballerini, L., Abbate, G., and Nistri, A. (2002) Experimental and modeling studies of novel bursts induced by blocking Na^+ pump and synaptic inhibition in the rat spinal cord. *J. Neurophysiol.* **88,** 676–691
56. Ballerini, L., Bracci, E., and Nistri, A. (1997) Pharmacological block of the electrogenic sodium pump disrupts rhythmic bursting induced by strychnine and bicuculline in the neonatal rat spinal cord. *J. Neurophysiol.* **77,** 17–23
57. Parker, D., Hill, R., and Grillner, S. (1996) Electrogenic pump and a Ca^{2+}-dependent K^+ conductance contribute to a posttetanic hyperpolarization in lamprey sensory neurons. *J. Neurophysiol.* **76,** 540–553
58. Brashear, A., Mulholland, G. K., Zheng, Q. H., Farlow, M. R., Siemers, E. R., and Hutchins, G. D. (1999) PET imaging of the pre-synaptic dopamine uptake sites in rapid-onset dystonia-parkinsonism (RDP). *Movement Disord.* **14,** 132–137
59. Simunovic, F., Yi, M., Wang, Y., Macey, L., Brown, L. T., Krichevsky, A. M., Andersen, S. L., Stephens, R. M., Benes, F. M., and Sonntag, K. C. (2009) Gene expression profiling of substantia nigra dopamine neurons: further insights into Parkinson's disease pathology. *Brain* **132,** 1795–1809
60. Sun, Y., Dong, Z., Khodabakhsh, H., Chatterjee, S., and Guo, S. (2012) Zebrafish chemical screening reveals the impairment of dopaminergic neuronal survival by cardiac glycosides. *PloS One* **7,** e35645
61. Baimbridge, K. G., Celio, M. R., and Rogers, J. H. (1992) Calcium-binding proteins in the nervous system. *Trends Neurosci.* **15,** 303–308
62. Seto-Ohshima, A. (1994) Review: calcium-binding proteins in the central nervous system. *Acta Histochem. Cytochem.* **27,** 93–106
63. Caillard, O., Moreno, H., Schwaller, B., Llano, I., Celio, M. R., and Marty, A. (2000) Role of the calcium-binding protein parvalbumin in short-term synaptic plasticity. *Proc. Natl. Acad. Sci. U.S.A.* **97,** 13372–13377
64. Benarroch, E. E. (2011) Na^+, K^+-ATPase Functions in the nervous system and involvement in neurologic disease. *Neurology* **76,** 287–293
65. Zugno, A. I., Stefanello, F. M., Streck, E. L., Calcagnotto, T., Wannmacher, C. M. D., Wajner, M., and Wyse, A. T. S. (2003) Inhibition of Na^+, K^+-ATPase activity in rat striatum by guanidinoacetate. *Int. J. Dev. Neurosci.* **21,** 183–189
66. Stöckler, S., Isbrandt, D., Hanefeld, F., Schmidt, B., and von Figura, K. (1996) Guanidinoacetate methyltransferase deficiency: The first inborn error of creatine metabolism in man. *Am. J. Hum. Genet.* **58,** 914–922